Electronic Supplementary Information

Strong size sieving effect in a rigid oxalate-based metal-organic framework for selective lithium extraction

Wenhao Huang [a], Zhonghang Chen [a], Peng Cheng [a] and Wei Shi [a]*

[a] Frontiers Science Center for New Organic Matter, Key Laboratory of Advanced Energy Materials Chemistry (MOE) and State Key Laboratory of Advanced Chemical Power Sources, College of Chemistry, Nankai University, Tianjin 300071, China.

* Corresponding author. E-mail address: shiwei@nankai.edu.cn (W. Shi)

Summary of the supporting information: 28 pages, 20 Figures and 2 tables.

Content

Experimental section

Synthesis

Synthesis of single crystals of Eu-C_2O_4. Eu-C_2O_4 was synthesized via an optimized method.[1] A mixture containing Eu_2O_3 (35 mg, 2.0 mmol), $H_2C_2O_4{\cdot}2H_2O$ (19 mg, 0.15 mmol), $NaHCO_3$ (27 mg, 0.30 mmol) and H_2O (4.0 mL) was transferred to a 20 mL glass vial and sonicated for 3 minutes. The reagent bottle was sealed and then heated at 90 °C for 2 h. After cooling to room temperature, the resulting colorless crystals were harvested by filtration, washed with H_2O and ethanol, and then dried at 70 °C. Yield 71% based on Eu_2O_3. Elemental analysis (%) for $EuC_2H_2O_6$: C 8.76, H 0.73, found (%): C 8.83, H 1.08.

Gram-scaled synthesis of powder Eu-C_2O_4. A mixture containing Eu_2O_3 (0.70 g, 2 mmol), $H_2C_2O_4{\cdot}2H_2O$ (0.38 g, 3 mmol), $NaHCO_3$ (0.54 g, 6 mmol) and H_2O (100 mL) was transferred to a 250 mL round-bottom flask and sonicated for 3 min. The flask was stirred under reflux for 2 h. After cooling to room temperature, the resulting colorless powder were harvested by filtration, washed with H_2O and ethanol, and then dried at 70°C. Yield 79% based on Eu_2O_3. Elemental analysis (%) for $EuC_2H_2O_6$: C 8.76, H 0.73; found (%): C 8.68, H 0.93.

Synthesis of Li@Eu-C_2O_4. A mixture containing $Eu(NO_3)_3{\cdot}6H_2O$ (0.088 g, 0.20 mmol), $H_2C_2O_4{\cdot}2H_2O$ (0.019 g, 0.15 mmol), Li_2CO_3 (0.022 g, 0.30 mmol), LiOH (0.012 g, 0.50 mmol), H_2O (2.0 mL) and DMF (2.0 mL) was transferred to a 15 mL pressure bottle. The bottle was sealed and then heated at 120 °C for 12 h. After cooling to room temperature, the resulting colorless crystals were harvested by filtration, washed withH_2O and ethanol, and then dried at 70 °C. Yield 68% based on $Eu(NO_3)_3{\cdot}6H_2O$. Elemental analysis (%) for $Li_2EuC_2O_6$: C 8.40, H 0; found (%): C 8.54, H 0.36.

Characterization

For single crystal X-ray diffraction, a single crystal was directly taken from the mother liquor and placed in paraffin oil. The crystal was mounted on a nylon loop and placed on the goniometer. Single-crystal data were collected using a Rigaku SuperNova or a Rigaku XtaLAB Mini II single-crystal diffractometer equipped with graphite-monochromatic Mo-Kα radiation (λ = 0.71073 Å). The crystal was kept at 293(2) K during data collection. The structures were solved by SHELXS (direct methods) and refined by SHELXL (full matrix least-squares techniques) in the Olex2 package.[2,3] All non-hydrogen atoms were refined anisotropically, while the hydrogen atoms were positioned geometrically and refined as riding atoms. PXRD measurements were performed using a Rigaku Smartlab SE X-ray diffractometer equipped with a Cu-tube and a graphite monochromator scanning over the range of 5–50° at the scan rate of 0.2° s^{-1} at room temperature. Simulations of the PXRD patterns were carried out with the single-crystal data and diffraction crystal module of the Mercury program. The FTIR spectroscopy were carried out on a Bruker ALPHA spectrophotometer. TGA data were obtained on a TGA 2 STARe System of METTLER TOLEDO under nitrogen atmosphere with the heating rate of 10 °C min^{-1}. EA for C, H and N were carried out using a Vario EL cube elemental analyzer. The SEM images were obtained using Hitachi SU3500 scanning electron microscopy equipped. ICP-AES analyses were conducted using a Thermo IRIS Advantage instrument. XPS were acquired using PHI5000Versa probe equipped ESCALAB 250xi.

Activation of Eu-C_2O_4

Before conducting adsorption experiments, as-synthesized Eu-C_2O_4 needs to be activated. The activation method is as follows. The material needs to be soaked in a nitric acid solution (pH = 3) at 80 °C for 12 hours, and fresh nitric acid solution should be replaced three times during the process. After cooling to room temperature, filter, wash with water and ethanol and dry at 70 °C.

DFT calculations

Computations were performed using Gaussian 16[4] with B3LYP/genecp+empirical dispersion correction GD3BJ. The mixed basis set is 6-311G* for H, C, O, Li, Na and SDD for Eu, respectively. Due to the limitations of the rigid framework, it can be assumed that structure of Na@Eu-C_2O_4 is the same as structure of Li@Eu-C_2O_4.

Kinetic adsorption studies

Kinetics experiments at 700 mg L^{-1} Li^+ by Eu-C_2O_4 were performed at 90 °C in 20 mL glass bottles. A Li^+ solution (10 mL, 700 mg L^{-1}) was added to each bottle, and 50 mg Eu-C_2O_4 was added to each bottle to form the suspension. The suspension was constantly stirred until 2 mL samples were collected at predetermined times (1 h, 3 h, 6 h, 9 h, 12 h, 18 h, 24 h and 36 h). Centrifuge each sample and dilute 1mL of the supernatant 100 times. Further analyze the sub samples using ICP-OES.

The adsorption capacity of lithium ions by Eu-C_2O_4 was determined via Equation (1):

$$q_t = \frac{C_0 - C_t}{m} \times V \qquad (1)$$

where C_0 (mg L^{-1}) and C_t (mg L^{-1}) are the concentrations of Li^+ before and after adsorption; m (g) is adsorbent mass and V(L) is the solution volume.

The pseudo-first-order kinetic and pseudo-first-order kinetic models were nonlinearly fitted with the experimental data via Equation (2) and Equation (3):

$$\ln(q_e - q_t) = \ln q_e - \frac{k_1}{2.303} \times t \qquad (2)$$

where q_e (mg g^{-1}) and q_t (mg g^{-1}) are the adsorption capacity of Li^+ at equilibrium and time t; t (h) is the adsorption time; k_1 (h^{-1}) is the pseudo-first-order kinetics adsorption rate constant.

$$\frac{t}{q_t} = \frac{1}{k_2 q_e^2} + \frac{t}{q_e} \qquad (3)$$

where q_e (mg g^{-1}) and q_t (mg g^{-1}) are the adsorption capacity of Li^+ at equilibrium and time t; t (h) is the adsorption time; k_2 (g mg^{-1} h^{-1}) is the pseudo-second-order kinetics adsorption rate constant.

Isotherm adsorption studies

Adsorption isotherms at 90 °C were obtained by stirring a suspension containing 50 mg of Eu-C_2O_4 and

10 mL of Li^+ solution at pH 12 using a heating magnetic stirrer at 100 rpm. The initial concentrations of Li^+ ranged from 100 to 700 mg L^{-1}. After stirring for 24 h, 2 mL samples were collected form each bottle and centrifuged. The concentrations of Li^+ in the supernatant were measured by ICP-OES.

The Langmuir and Freundlich isotherm models were nonlinearly fitted with the experimental data via Equation (4) and Equation (5):

$$q_e = \frac{q_m K_L C_e}{1 + K_L C_e} \quad (4)$$

where q_e (mg g^{-1}) is the amount of Li^+ adsorption capacity at equilibrium; C_e (mg L^{-1}) is the residual concentration of Li^+ at equilibrium; q_m (mg g^{-1}) is the maximum adsorption capacity of the adsorbent at equilibrium and K_L (L mg^{-1}) is the Langmuir affinity constant.

$$q_e = K_F C_e^{1/n} \quad (5)$$

where q_e (mg g^{-1}) is the amount of Li^+ adsorption capacity at equilibrium; C_e (mg L^{-1}) is the residual concentration of Li^+ at equilibrium; K_F (mg g^{-1})(L mg^{-1})$^{1/n}$ is the Freundlich affinity constant.

Recyclability of adsorbents

The recyclability of the Eu-C_2O_4 was investigated by adsorption-desorption experiments repeated for several times (add 50 mg Eu-C_2O_4 into 10 mL Li^+ solution, pH = 12, 90 °C, C_0 = 700 mg L^{-1}). After adsorption equilibrium, centrifuge the supernatant ,dilute and measure the Li^+ concentration via ICP-OES, and the adsorbent is collected by filtration. The collected adsorbent was regenerated by acid treatment with HNO_3 (pH = 3) for 12 h and then washed with deionized water for reuse.

Adsorption selectivity

To determine the selectivity of the adsorbents, the mixed ion solution of Li^+ and Na^+ (Li^+ 700 mg L^{-1}, Na^+ 2300/6900/23000 mg L^{-1}, pH = 12, 90 °C) was used for competitive adsorption experiments. The ion concentrations were determined by ICP-OES and the ability of selective adsorption could be reflected by separation factors of different reference ions in a two-component system using Equation (6) and Equation (7):

$$K_d = \frac{(C_0 - C_e)V}{C_e m} \quad (6)$$

$$\alpha_{Na}^{Li} = \frac{K_{d,Li}}{K_{d,Na}} \quad (7)$$

where C_0 (mg L^{-1}) is the initial concentration of M^+; C_e (mg L^{-1}) is the residual concentration of M^+ at equilibrium; V (mL) is the volume of solution; m (mg) is the adsorbent mass; K_d is the parameter related to the adsorption capacity; and α_{Na}^{Li} is the parameter representing selectivity.

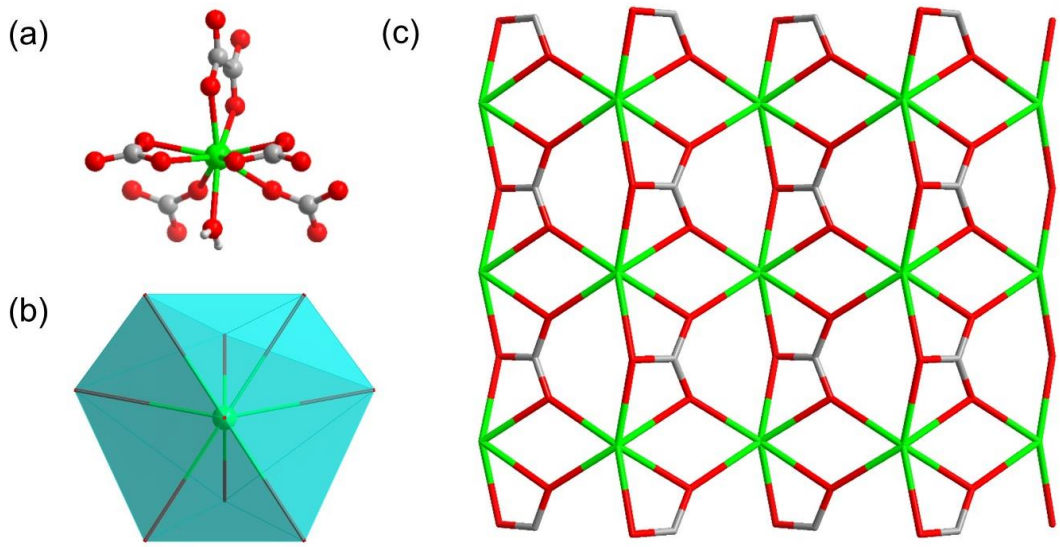

Fig. S1. (a) Coordination configuration, (b) coordination polyhedron and (c) 2D layer structure of Eu-C_2O_4.

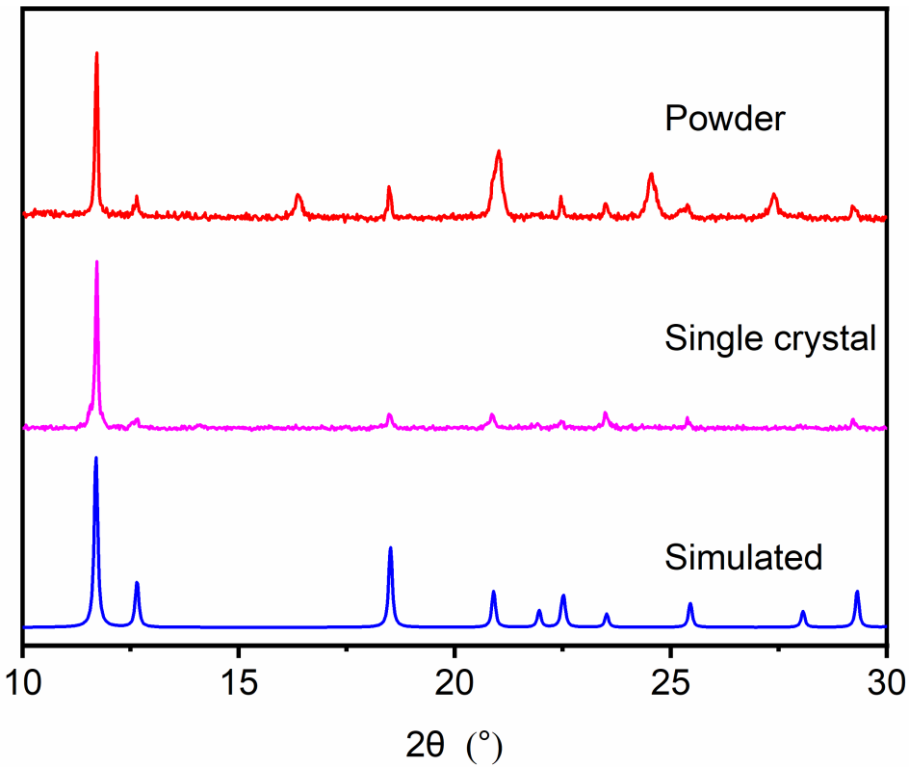

Fig. S2. PXRD patterns of Eu-C_2O_4.

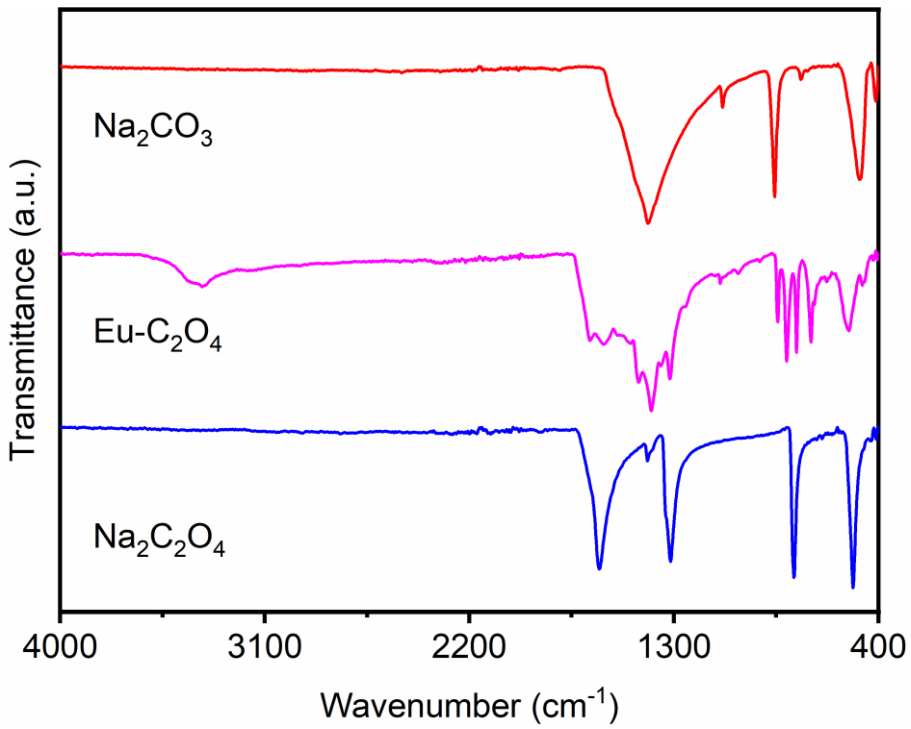

Fig. S3. IR spectra of Eu-C_2O_4, oxalate and carbonate.

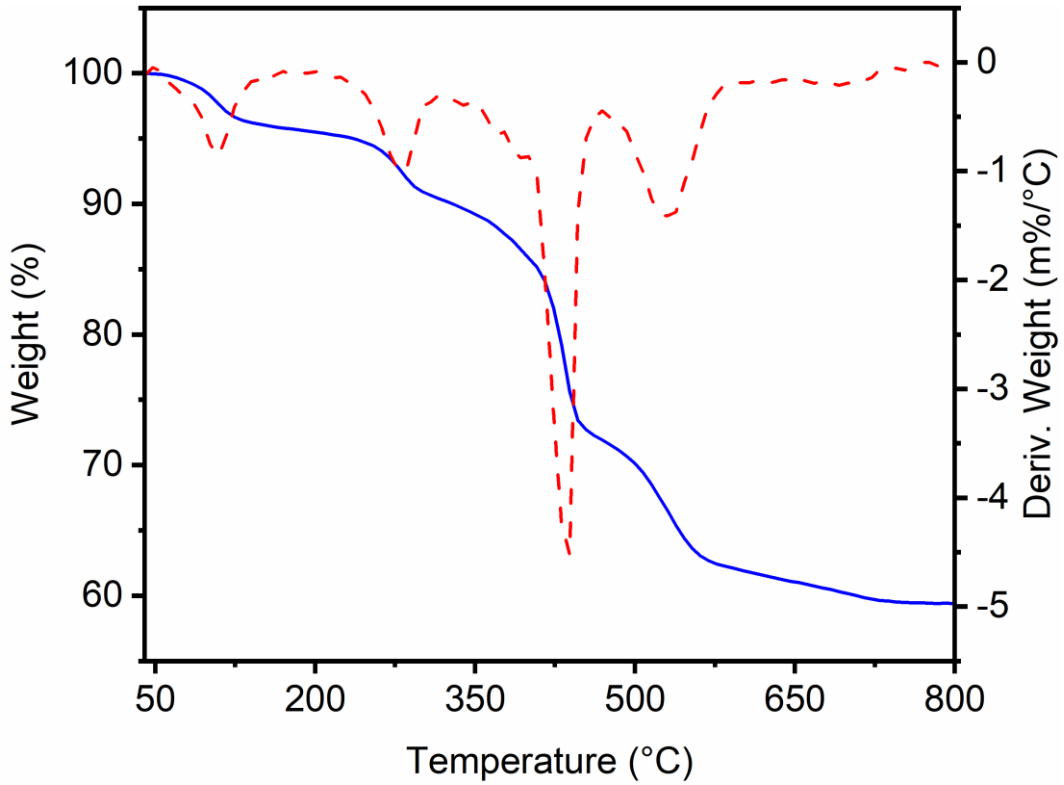

Fig. S4. TGA and DTG curves of Eu-C_2O_4.

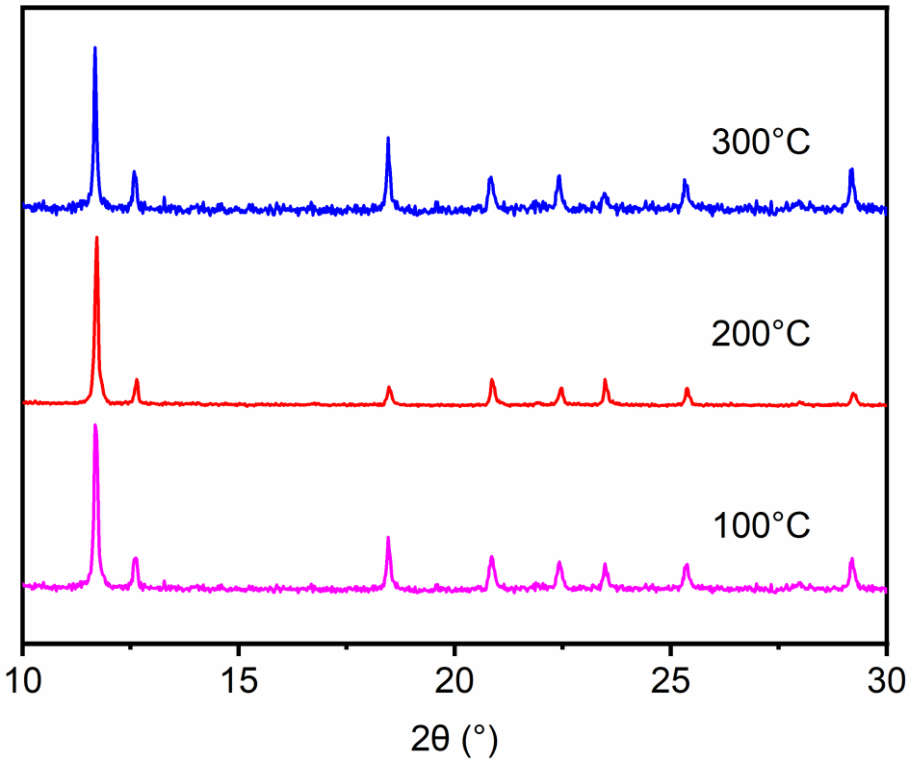

Fig. S5. Temperature-dependent PXRD patterns of Eu-C_2O_4.

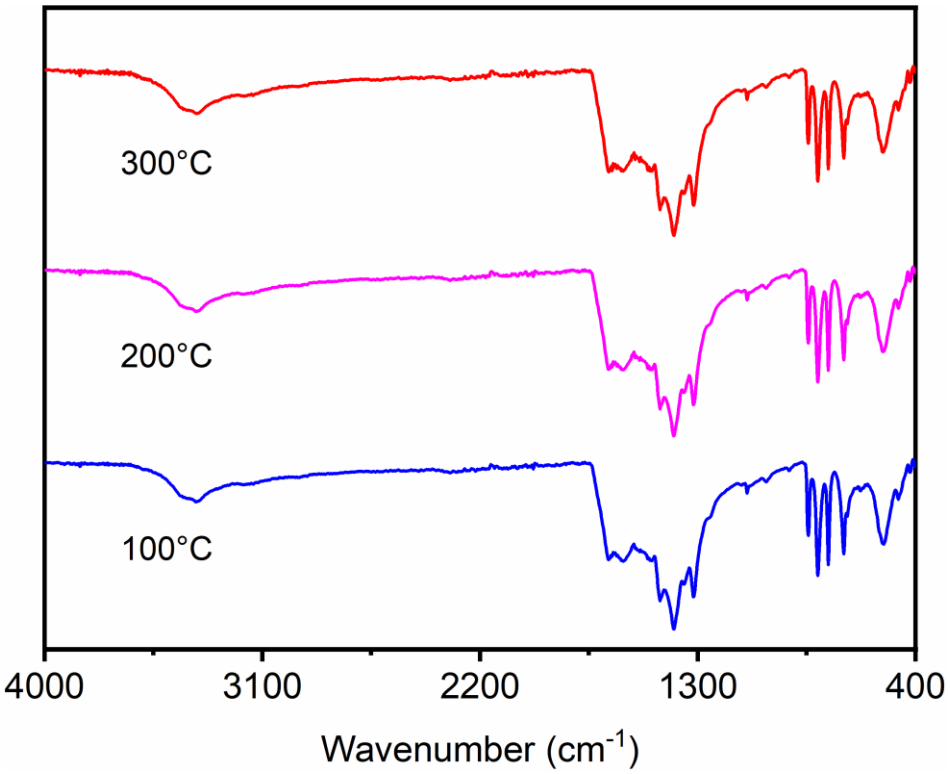

Fig. S6. Temperature-dependent IR spectra of Eu-C_2O_4.

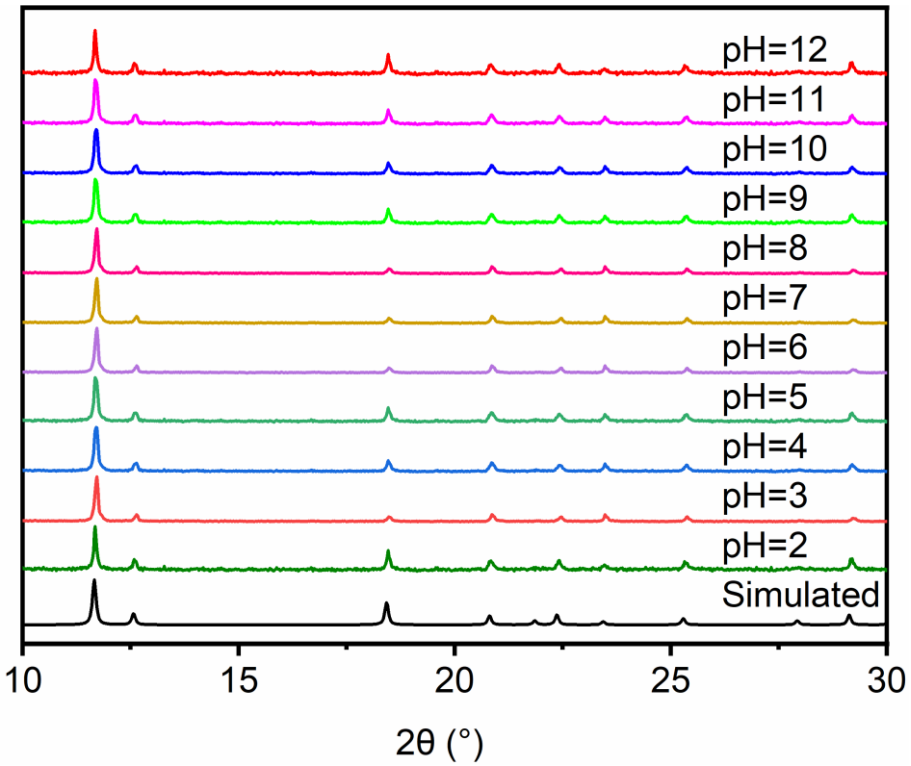

Fig. S7. PXRD patterns of Eu-C_2O_4 after 12 h in aqueous solutions with pH values ranging from 2 to 12.

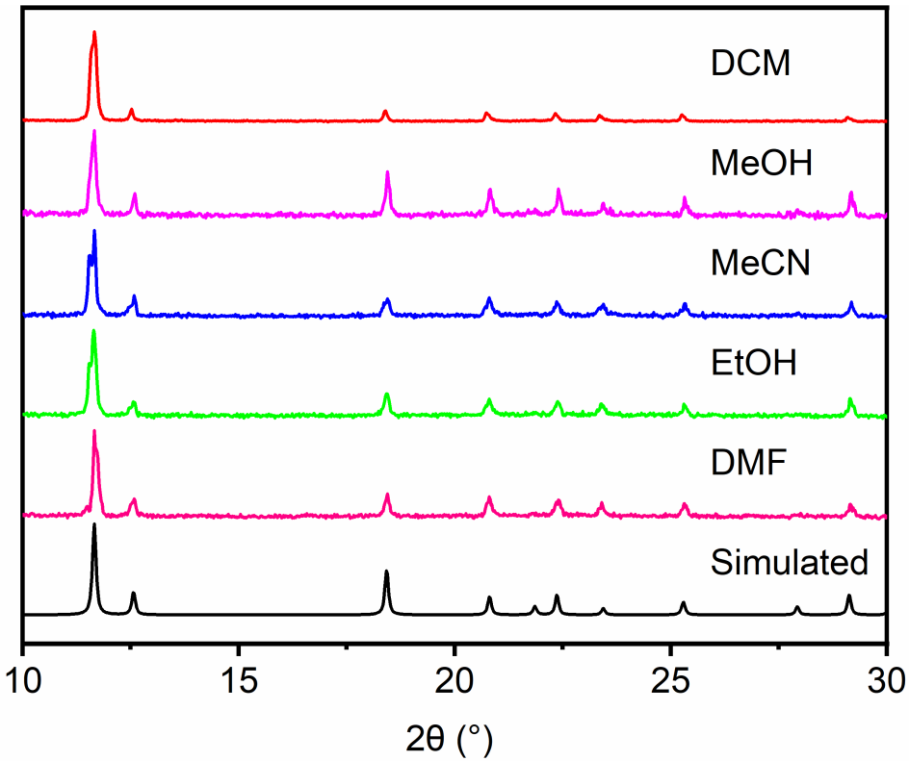

Fig. S8. PXRD patterns of Eu-C_2O_4 after 24 h in different organic solutions.

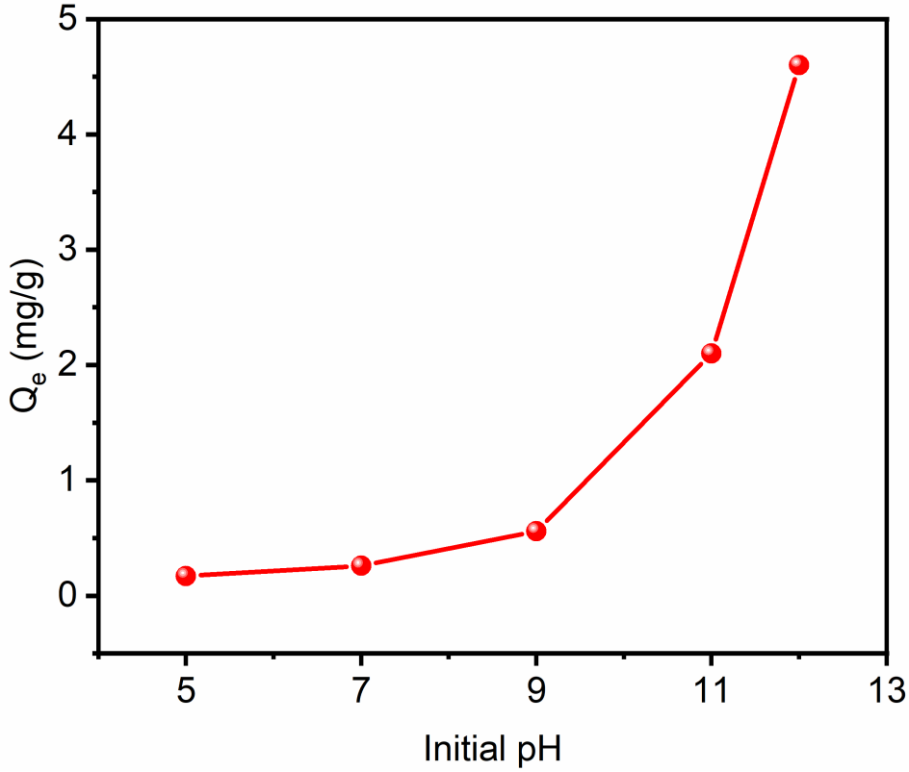

Fig. S9. The effect of initial pH on Li^+ adsorption capacity.

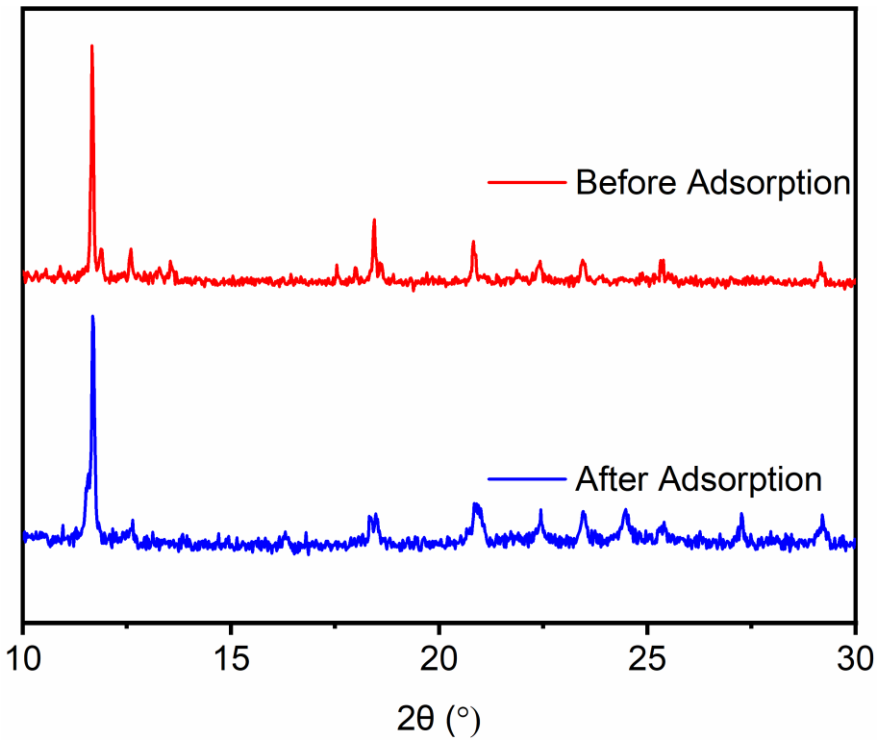

Fig. S10. PXRD patterns of Eu-C_2O_4 before and after adsorption of Li^+ ions.

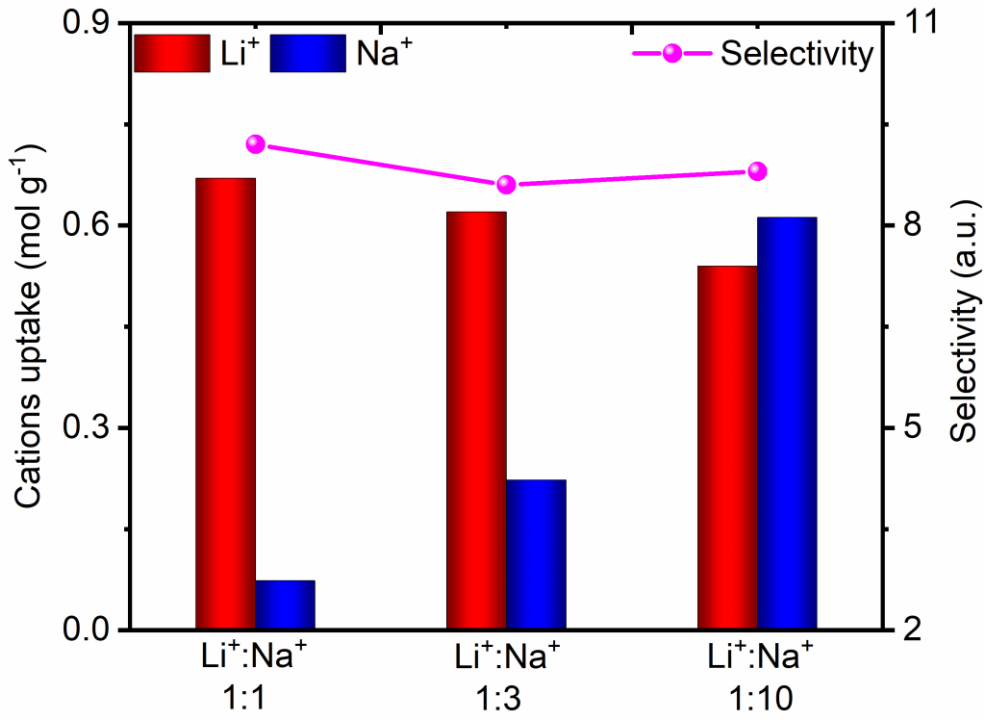

Fig. S11. Li^+ adsorption selectivity from the coexisting cations solution.

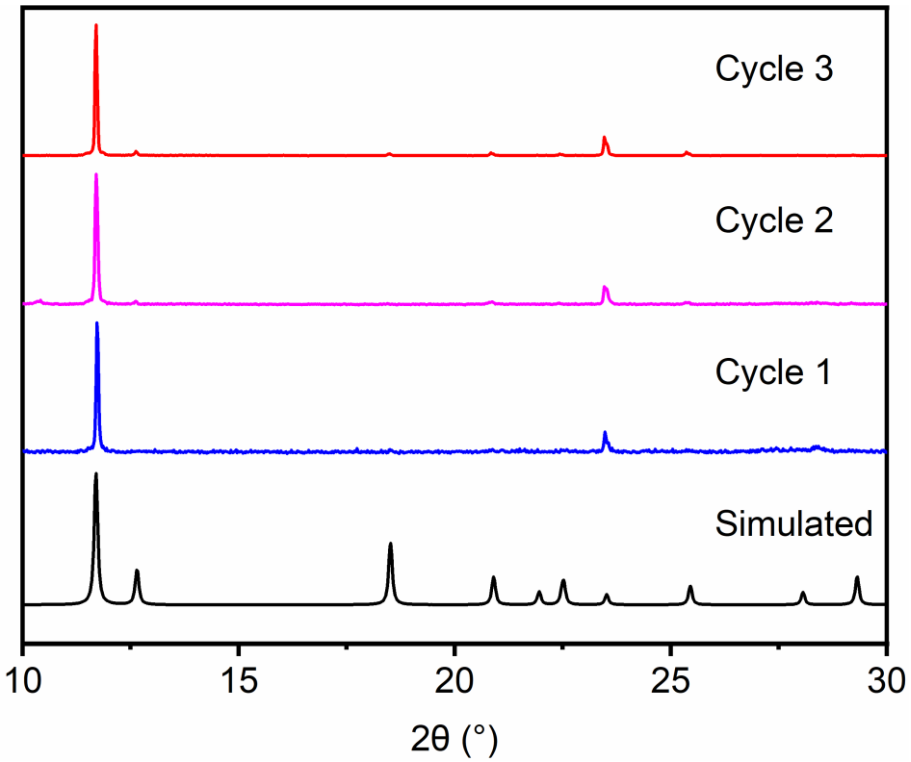

Fig. S12. PXRD patterns of Eu-C_2O_4 in regeneration cycle.

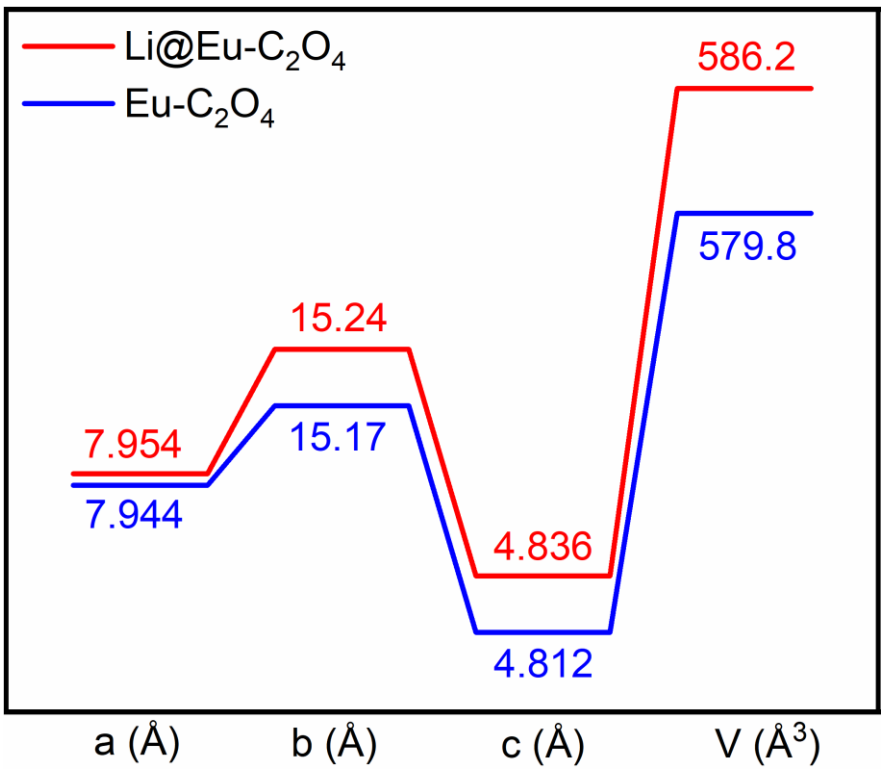

Fig. S13. Comparison of crystal cell parameters of Li@Eu-C_2O_4 and Eu-C_2O_4.

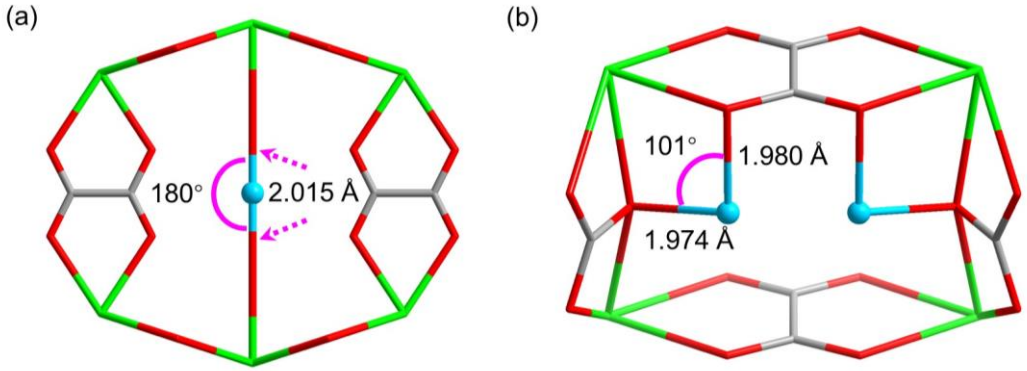

Fig. S14. Coordination configurations of Li^+ ions in Li@Eu-C_2O_4.

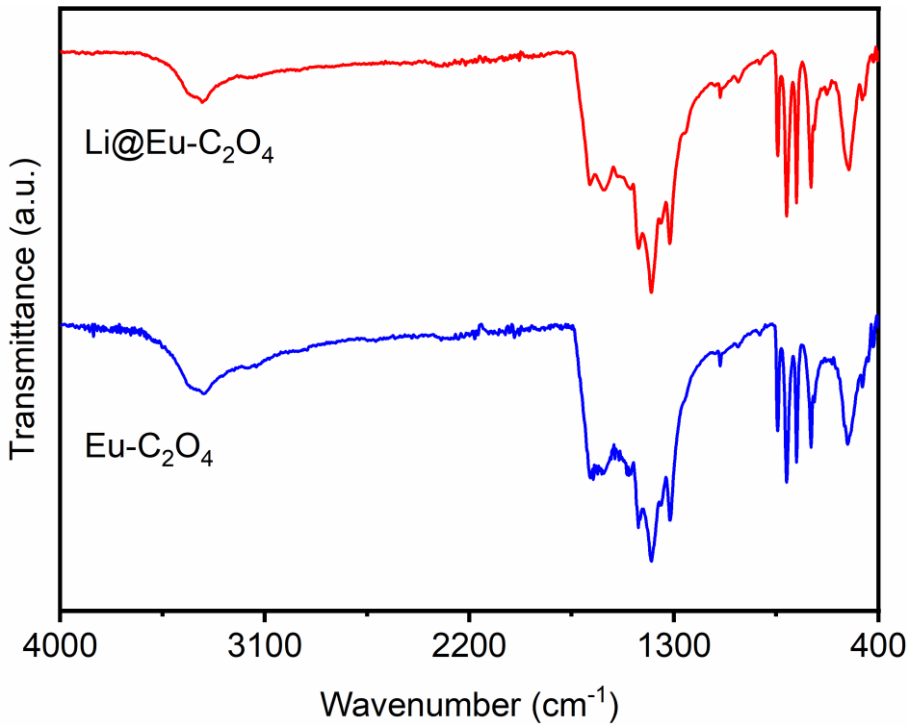

Fig. S15. IR spectra of Eu-C_2O_4 and Li@Eu-C_2O_4.

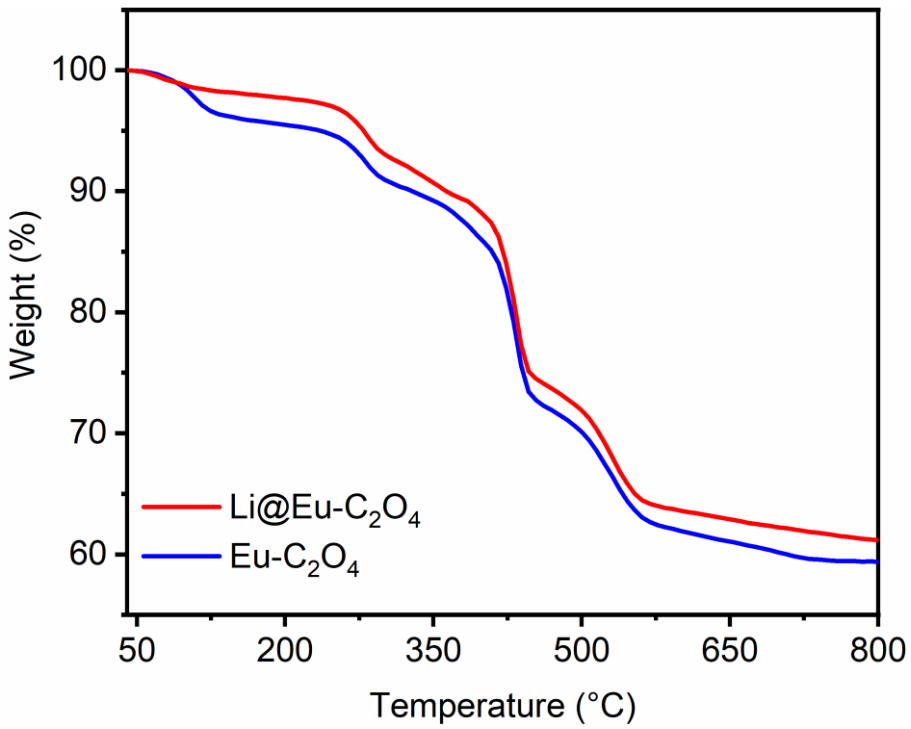

Fig. S16. TGA curves of Eu-C_2O_4 and Li@Eu-C_2O_4.

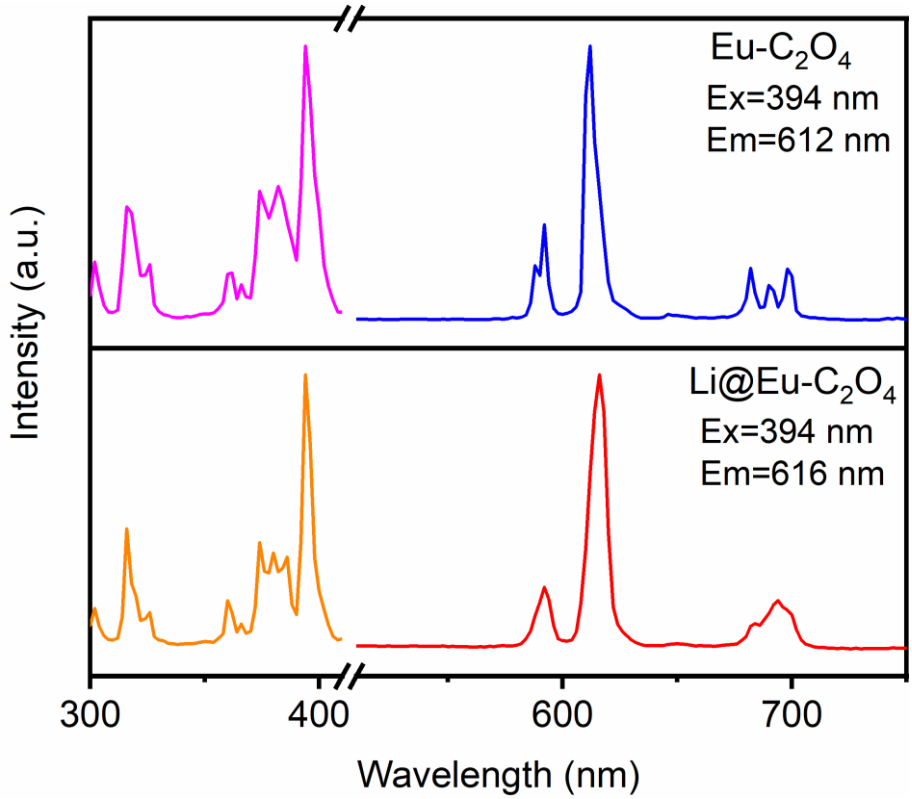

Fig. S17. Solid-state excitation and emission spectra of Li@Eu-C_2O_4 and Eu-C_2O_4.

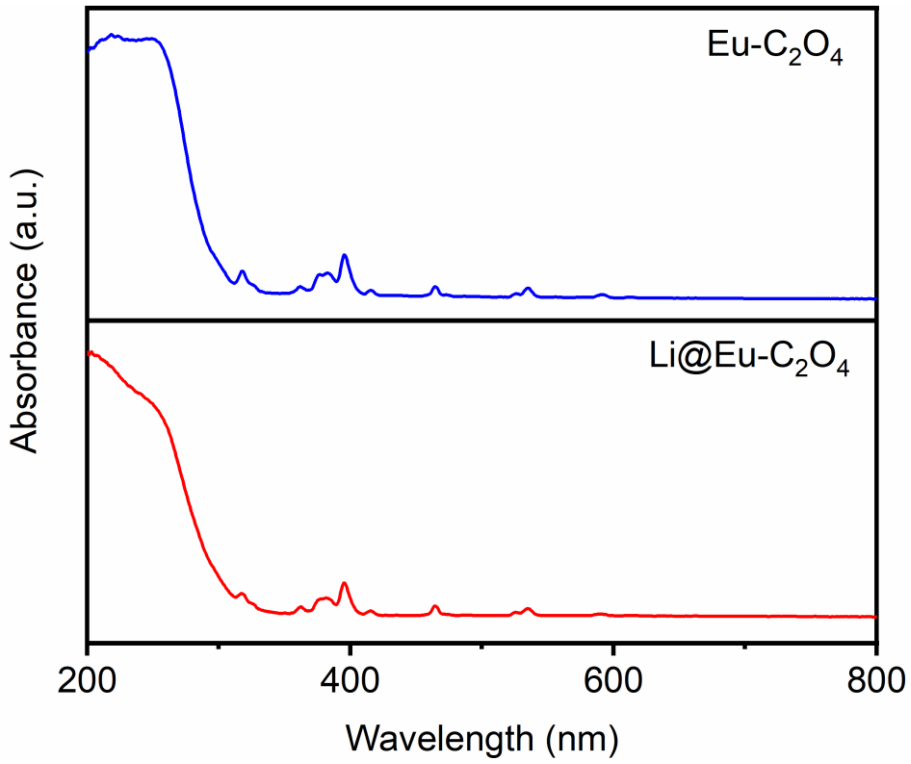

Fig. S18. Solid-state UV-vis spectra of Li@Eu-C_2O_4 and Eu-C_2O_4.

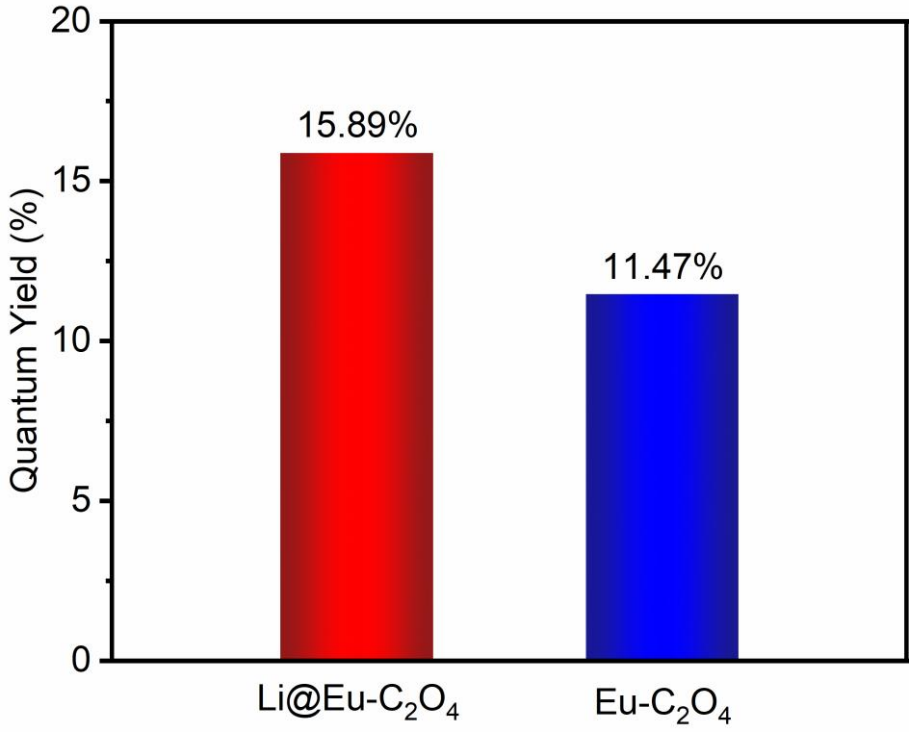

Fig. S19. Quantum yield of Li@Eu-C_2O_4 and Eu-C_2O_4.

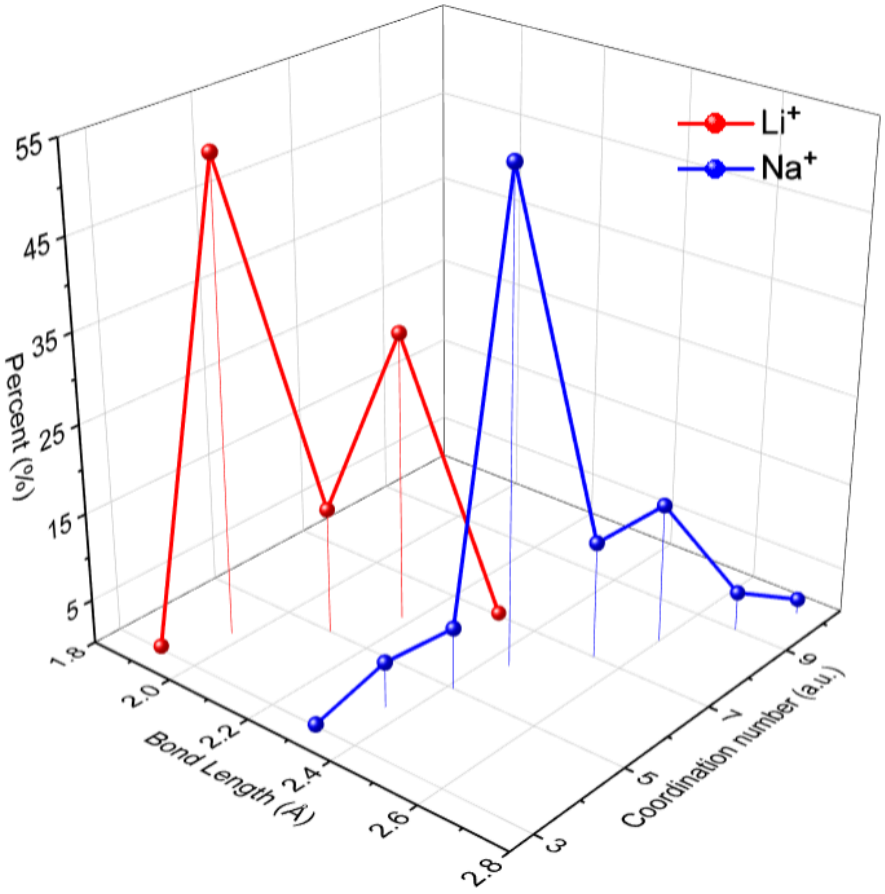

Fig. S20. Bond-length statistics for Li^+ and Na^+.[5]

Table S1. Crystal Data and Structure Refinement for Eu-C_2O_4 and Li@Eu-C_2O_4.

	Eu-C_2O_4	Li@Eu-C_2O_4
Formula	$EuC_2H_2O_6$	$Li_4Eu_2C_4O_{12}$
Formula weight	273.99	285.86
Crystal system	Orthorhombic	Orthorhombic
Space group	*Cmmm*	*Cmmm*
a / Å	7.9438(8)	7.9539(8)
b / Å	15.1693(16)	15.2398(13)
c / Å	4.8115(4)	4.8359(4)
α / deg	90	90
β / deg	90	90
γ / deg	90	90
V / Å^3	579.79(10)	586.19(9)
Z	4	2
ρ_{calc} / g cm^{-3}	3.139	3.239
μ / mm^{-1}	10.776	10.66
Reflections collected	1116	1184
Independent reflections	375	379
R(int)	0.0284	0.0383
2ϑ range / deg	5.370 to 52.996	5.346 to 52.952
F(000)	500.0	516.0
GOF on F^2	1.082	1.138
[a]R_1 / [b]wR_2[$I \geq 2\sigma$ (I)]	0.0271 / 0.0617	0.0339 / 0.0903
[a]R_1 / [b]wR_2 (all data)	0.0300 / 0.0625	0.0398 / 0.0948
Largest diff. peak / hole / eÅ^{-3}	1.71/-1.66	1.46/-2.92

[a]$R_1 = \sum||F_o| - |F_c||/\sum|F_o|$. [b]$wR_2 = [\sum w(F_o^2 - F_c^2)^2/\sum w(F_o^2)^2]^{1/2}$.

Table S2. Comparison of the selected adsorbing materials for Li^+ ions.

Materials	Li^+ uptake (mg g^{-1})	Equilibration time (h)	pH and Li^+ Concentration	Li^+ density (nm^{-3})	Selectivity of Li^+/Na^+	Reference
Eu-C_2O_4	**4.6**	**18**	**pH = 12, 700 mg L^{-1}**	**3.41**	**9.1**	**This work**
LMOF-321	7.5	24	pH = 7, 10 mg L^{-1}	0.44	6.2	6
UIO-66-H_2/H_4	39.5	1	pH = 6, 500 mg L^{-1}	0.89	1.95	7
TJU-21	41	16	pH = 7, 1000 mg L^{-1}	0.72	5.4	8
MIL-100(Fe)	46.3	24	pH = 7, 2000 mg L^{-1}	0.92	3.3	9
PDMVBA-MIL-121	1.4	24	pH = 7, 1000 mg L^{-1}	2.73	2.1	10
WP@PSS@Cu-MOF	8.9	3	pH = 9, 150 mg L^{-1},	—	2.4	11
pNCE/MOF-808	0.05	10	pH = 7, 700 mg L^{-1}	—	0.05	12
H_2TiO_3	28	1.5	pH = 12, 280 mg L^{-1}	37.47	—	13
HTO-PVB	25	3	pH = 12, 200 mg L^{-1}	—	93.5	14
$H_{1.6}Mn_{1.6}O_4$	43.8	2	pH = 11, 150 mg L^{-1}	11.47	—	15
HMZO	24.8	1.5	pH = 6, 130 mg L^{-1}	—	47.6	15
HMZO-PVC	18.3	4	pH = 6, 35 mg L^{-1}	—	55.3	16
$HAlSi_2O_6$	29.6	24	pH = 12, 300 mg L^{-1}	11.3	21.2	17

Li^+ Density refers the number of Li^+ ions can be adsorbed per unit volume of adsorbent.

References

1. R. Takono, T. Ishida, B. Ay, *CrystEngComm*, 2022, **24**, 7786–7792.
2. G. M. Sheldrick, *Acta Crystallogr., Sect. A: Found. Crystallogr.*, 2008, **64**, 112–122.
3. G. M. Sheldrick, *Acta Crystallogr., Sect. C: Struct. Chem.* 2015, **71**, 3–8.
4. M. J. Frisch, G. W. Trucks, H. B. Schlegel, G. E. Scuseria, M. A. Robb, J. R. Cheeseman, G. Scalmani, V. Barone, G. A. Petersson, H. Nakatsuji, X. Li, M. Caricato, A. V. Marenich, J. Bloino, B. G. Janesko, R. Gomperts, B. Mennucci, H. P. Hratchian, J. V. Ortiz, A. F. Izmaylov, J. L. Sonnenberg, D. Williams-Young, F. Ding, F. Lipparini, F. Egidi, J. Goings, B. Peng, A. Petrone, T. Henderson, D. Ranasinghe, V. G. Zakrzewski, J. Gao, N. Rega, G. Zheng, W. Liang, M. Hada, M. Ehara, K. Toyota, R. Fukuda, J. Hasegawa, M. Ishida, T. Nakajima, Y. Honda, O. Kitao, H. Nakai, T. Vreven, K. Throssell, J. J. A. Montgomery, J. E. Peralta, F. Ogliaro, M. J. Bearpark, J. J. Heyd, E. N. Brothers, K. N. Kudin, V. N. Staroverov, T. A. Keith, R. Kobayashi, J. Normand, K. Raghavachari, A. P. Rendell, J. C. Burant, S. S. Iyengar, J. Tomasi, M. Cossi, J. M. Millam, M. Klene, C. Adamo, R. Cammi, J. W. Ochterski, R. L. Martin, K. Morokuma, O. Farkas, J. B. Foresman, D. J. Fox, Gaussian 16, Revision A.03, Gaussian, Inc., Wallingford CT, 2016.
5. O. C. Gagné, F. C. Hawthorne, *Acta Crystallogr., Sect. B: Struct. Sci.*, 2016, **72**, 602–625.
6. N. D. Rudd, Y, Liu, K. Tan, F. Chen, Y. J. Chabal, J. Li, *ACS Sustainable Chem. Eng.*, 2019, **7**, 6561−6568.
7. X. Gao, R. Ding, H. Huang, B. Liu, X. Zhao, *Chem. Commun*., 2023, **59**, 13183–13186.
8. X. Jiang, B. Wu, P. Bai, J. Lyu, X. Guo, *ACS Appl. Mater. Interfaces*, 2021, **13**, 47793–47799.
9. B. Tong, G. Guo, X. Meng, P. Bai, J. Lyu, X. Guo, *Chem. Commun.*, 2022, **58**, 8866-8869.
10. R. Ou, H. Zhang, J. Wei, S. Kim, L. Wan, N. S. Nguyen, Y. Hu, X. Zhang, G. P. Simon, H. Wang, *Adv. Mater.*, 2018, **30**, 1802767.
11. W. Bian, J. Chen, Y. Chen, W. Xu, J. Jia, *Cellulose*, 2021, **28**, 3041-3054.
12. S. Zhang, R. Ou, H. Ma, J. Lu, M. M. B. Holl, H. Wang, *Chem. Eng. J.*, 2021, **405**, 127037.
13. Y. Zhang, J. Liu, Y. Yang, S. Lin, P. Li, *Sep. Purif. Technol.*, 2021, **267**, 118613.
14. F. Qian, M. Guo, Z. Qian, Q. Li, Z. Wu, Z. Lin, *Chem. Eur. J.*, 2019, **4**, 10157–10163.
15. Wang, L.; Wang, L.; Wang, J.; Wang, X. *Sep. Purif. Technol.*, 2022, **303**, 121933.
16. L. Wang, L. Wang, J. Wang, X. Wang, *Sep. Purif. Technol.*, 2022, **303**, 121933.
17. H. Hu, J. Guo, M. Liu, Y. Li, N. Wu, L. Xiong, S. Chen, B. Tian, L. Zhuang, *Hydrometallurgy*, 2022, **213**, 105929.